Results in Engineering 30 (2026) 110781

Contents lists available at ScienceDirect

Results in Engineering

journal homepage: www.sciencedirect.com/journal/results-in-engineering

Research paper

Design of pH-dependent ZnO-reinforced electrospun poly(ethylene furanoate)/poly(3-hydroxybutyrate) nanofibrous membranes for sustainable food packaging

James Kegere [a,c], Athira V. Aramughan [b], Anuj Niroula [b], Bismi Phasaludeen [b], Akmal Nazir [b,*], Ioannis Zuburtikudis [c,*], Muhammad Z. Iqbal [a,*]

[a] Department of Chemical and Petroleum Engineering, College of Engineering, United Arab Emirates University, Al Ain, United Arab Emirates
[b] Department of Food Science, College of Agriculture and Veterinary Medicine, United Arab Emirates University, Al Ain, United Arab Emirates
[c] Department of Chemical Engineering, College of Engineering, Abu Dhabi University, Abu Dhabi, United Arab Emirates

ARTICLE INFO

Keywords:
Poly(ethylene furanoate)
Poly(3-hydroxybutyrate)
Nanofiber composites
Zinc oxide
Electrospinning
Release kinetics

ABSTRACT

We report on the manufacturing of 100% biorenewable co-electrospun membranes from poly(ethylene furanoate) (PEF) and poly(3-hydroxybutyrate) (PHB), loaded with ZnO, for food packaging applications. Co-solutions of both polymers were electrospun into nonwoven mats, and the impact of ZnO incorporation on the physical, chemical, and barrier properties was evaluated. The PEF/PHB nonwoven mats, though immiscible, revealed no phase separation when in the form of fibers. Added ZnO stabilized the co-spun nanofibers by interacting with hydroxyl groups, forming stabilized interactions that led to the entrapment of Zn^{2+} within the mat, tunable with the films' pH. Inclusion of ZnO in PEF/PHB improved the mechanical strength of the nonwoven mats by ~77% and 70% in Young modulus and tensile strength, respectively. Water vapor transmission through the nonwoven mats was reduced with ZnO after 24 h (0.3 g day^{-1} from 0.4 g day^{-1}). Furthermore, the release of entrapped Zn^{2+} in the blend nonwoven mats was investigated via response surface methodology as a function of temperature, pH, and time. Our results reveal that PEF/PHB+ZnO nonwoven mats disentangle to release trapped Zn^{2+} at low pH and high temperature, whereas low temperature and basic conditions force compaction, decreasing Zn^{2+} release.

1. Introduction

The food packaging industry has long been dominated by synthetic plastics owing to their low cost and durability. However, environmental pollution is a serious side effect emerging from this wide use of synthetic polymers [1–3]. A shift towards bio-renewable counterparts to synthetic polymers is currently being implemented by several governments, banning the use of single-use plastics. Some commonly used replacements for polyolefins are polyhydroxybutyrate (PHB) and polylactic acid (PLA), and more recently, poly(ethylene furanoate) (PEF) is highly regarded replacement for poly(ethylene terephthalate) (PET). PEF exhibits low melting temperature, high gas barrier, and higher glass transition temperature compared to PET [4], and being 100% bio-renewable, PEF is more suitable in manufacturing environmentally friendly food packaging materials [5].

PHB is the most widely used polymer from the PHAs with configuration and properties similar to polypropylene (PP), and as a result, is a promising candidate to substitute polypropylene in the manufacture biodegradable plastics. These properties emanate from high stereo-regularity in PHB leading to highly crystalline structure with degree of crystallinity up to 70–75%. Despite advantages of sustainability and end-of-life compostability, high production cost and brittleness in pure form limit PHB's industrial adaptability. For example, Olejnik et al. [6] reported <10% elongation at break (ε_b) for PHB films with tensile strength of ~10 MPa, which is low compared to polyolefins. On the other hand, PEF is 100% bio-based, and it exhibits good thermal properties, and higher gas barrier compared to PET, making it an ideal material for packaging applications [O_2~11x, CO_2~19x, and H_2O~2.8x compared to PET] [7]. Structurally, the presence of furan-ring, absence of ring-flipping, presence of low bond-angles in the carboxylic side groups, and the dipole moments on the furan-ring result in higher barrier performance of PEF [7]. Similar to PHB, PEF is brittle in pure form

* Corresponding authors.
E-mail addresses: akmal.nazir@uaeu.ac.ae (A. Nazir), ioannis.zuburtikudis@adu.ac.ae (I. Zuburtikudis), mziqbal@uaeu.ac.ae (M.Z. Iqbal).

https://doi.org/10.1016/j.rineng.2026.110781
Received 3 February 2026; Received in revised form 24 April 2026; Accepted 28 April 2026
Available online 30 April 2026
2590-1230/© 2026 The Author(s). Published by Elsevier B.V. This is an open access article under the CC BY license (http://creativecommons.org/licenses/by/4.0/).

(ε_b ~2–4%) [8].

Electrospinning is a scalable technique to produce ultrafine micro- and nanofibers from polymer solutions under a high-voltage electric field. Electrospinning generates nonwoven mats with high surface area, porosity, and mechanical strength; all valuable for advanced food packaging applications. Electrospun nanofibers can serve as active, intelligent packaging and as edible films with high gas and UV barriers, outperforming conventional cast films for similar applications [9]. Brittle polymers show reasonable mechanical properties when electrospun compared to molding or cast films. For example, glass fiber cast films exhibit extreme brittleness and no flexibility, whereas electrospun glass fiber wool has an average ε_b of ~8.7% [10]. Similarly, Del Gaudio et al. [11] reported PCL/poly(3-hydroxybutyrate-co-3-hydroxyvalerate) (PHBV) blends with an elastic modulus of 1300 ± 250 MPa and ε_b~3 ± 1% in solvent cast PHBV films. On the other hand, electrospun mat of PHBV showed an elastic modulus of 77 ± 15 MPa and ε_b of 30 ± 20%. Nevertheless, these examples fortify the idea that brittleness in polymer films could be reduced if processed via electrospinning but at the cost of overall strength of the polymers which is still acceptable according to food-packaging standards [12].

Being a new polymer in the market, there are less reports on evaluating mechanical properties of PEF. Ding et al. [13] reported a tensile strength of 52.5 MP, modulus of 65 MPa, and ε_b<3% for solvent cast PEF films. Ahmed et al. [14] recently reported a tensile strength of 34.7 MPa, modulus of 190 MPa, and a strain at break of 2.4% in melt-extruded PEF, which are markedly different than the results from Ding et al. On the other hand, Kandiyil et al. [15] performed electrospinning of PEF/PLA blends to produce membranes for oil-water emulsions. They reported a modulus of 16 MPa and 62% strain at break which is remarkably higher compared to what was observed in solvent cast and melt-extruded PEF films.

Nanoparticle-loaded electrospun fibers contain additional properties, such as manufacturing smart packaging films with controlled release of nanoparticles with active strains. ZnO nanoparticles are known to impart active properties to the packaging materials. Though ZnO-stabilized nanofibers are common, not many studies have investigated potential encapsulation and release behavior of ZnO. In this respect, release of ZnO might be influenced by chemical interaction with the encapsulating matrix, pH of surrounding medium, temperature, and, most importantly, time. Due to covalent interactions in many composite films, ZnO release is highly limited, making the interaction with microbes localized at the surface. In other cases, there have been reports of minimal to steady release of ZnO nanoparticles from electrospun membranes. Jebel et al. [16] studied the release of ZnO from cellulose films and their findings show an initial burst release followed by a steady release profile for several days. A study conducted by Amjadi et al. [17] on the effect of ZnO nanoparticles in gelatin and chitosan-based nanofibers reveals the effect of slow release on the antibacterial activity of fibers, where Zn interaction with the microorganism was limited due to agglomeration.

In this work, co-electrospinning of PEF and PHB (with ZnO) solution was performed to produce nanofiber nonwoven mats with the hypothesis of increased ε_b and strength at the same time since both polymers are immiscible. It is worth noting that there are no published reports on PEF/PHB electrospun blends, and hence, it is difficult to benchmark the outcomes. The effect of ZnO on the thermomechanical and water barrier properties of PEF/PHB nonwoven mats was investigated. In addition, the mechanism of ZnO-polymer interaction leading to the release or confinement of Zn^{2+} from the mats is reported. This work sheds light on the active/inactive behaviors of ZnO-loaded food-preservation packaging films.

2. Materials and methods

2.1. Materials

Trifluoracetic acid (TFA, 99%, Pcode:102,285,924, Lot#STBJ7788), and Zinc Oxide nanopowder (<100 nm) MKCQ9923 were purchased from signal Aldrich (USA), polyhydroxybutyrate (PHB) (grade ENMAT Y3000P) was acquired in form of pellets from Tianan Biologic materials (Zhejiang China), and Poly (ethylene furanoate) (PEF) with a MW >30,000 g/mol and intrinsic viscosity of >0.5 g/mL were purchased from Avantium, Netherlands.

2.2. Preparation of co-spun nanofibers

Solutions of PEF (10% w/w) and PHB (10% w/w) in TFA were prepared separately (6 h stirring at room temperature). The two solutions were then blended in different weight ratios (1:1, 2:1, 3:2, and 2:3) and stirred magnetically at room temperature for 6 h at 400 rpm. ZnO (1 wt% relative to the polymer content) was added to the prepared PEF/PHB (1:1) polymer solution, and the mixture was sonicated at room temperature for 30 min. The dispersion of ZnO in PEF/PHB solutions was analyzed via point-laser to check the presence of any flakes or unmixed particles. No flakes or chunks were observed.

10 mL of as-prepared (PEF/PHB, PEF/PHB+ZnO) solutions in 20 mL syringes were mounted on a pump connected to an electrospinner (EFIBER F300, SKe Research, Italy). The spinneret (20 G, ID/OD: 0.584/0.889 mm/mm) attached to the syringe through a silicone tube was connected to a high-voltage power source via crocodile clips using a direct current supply unit. After adjusting the working parameters (19 kv, 1 mL/h, collector distance ~ 13 cm), electrospinning was conducted as illustrated in Scheme 1 for 10 h. The fibers were collected on a rotating drum collector at 500 rpm, covered with aluminum foil. The nonwoven mats were collected by detaching from the aluminum foil, dried in an oven for 6 h at 65 °C. The dispersion of ZnO nanoparticles in PEF/PHB mats was examined using Electron Dispersive Spectroscopy (EDS) (Fig. S1).

2.3. Characterization techniques

Nonwoven mats were cut into 1cm^2 sheets, sputter-coated with gold, and imaged using a scanning electron microscope (Thermoscientific Quattro ESEM). X-ray diffraction (XRD) spectra were obtained using Rigaku MiniFlex benchtop XRD, fitted with a CuK radiation tube (λ = 1.542 Å), operating at 40 kV and 2° min^{-1} scan rate in 2θ range 5–80° Fourier Transform Infra-red (FTIR) spectra were collected using a Thermo Nicolet Nexus 470 FTIR spectrophotometer. Nonwoven mats were cut into very fine pieces using a manual cutting blade, ground in KBr window, and pelleted by a hydraulic press. 32 scans were conducted in the frequency range 400–4000 cm^{-1}, and spectra were corrected for CO_2. Thermal stability was investigated using a thermogravimetric analyzer (Shimadzu TGA-50 analyzer). Approximately 10 mg of the sample was heated from 35 to 800 °C at 10 °C per minute. For the wettability test, straight chunks of nonwoven mats were firmly placed on a glass slide, and a custom-built setup was used to mount a single water droplet through a syringe using a controlled flow pump. A digital camera was used to image the droplet, and further, the contact angles were ascertained using Image J. Mechanical properties were studied using a universal testing machine (Shimadzu AG-X 10KN). Samples were cut into rectangular shapes with a thickness of 0.1 mm, a 60 mm gap, and an overhead speed of 1mm/minute.

2.4. Water barrier performance

A water barrier test was carried out following Kurabetta et al. [18] and Bhat et al. [19] with slight modification. Nonwoven mats (200 μm) were cut into 30 × 30 mm2 squares, covering a weighing bottle

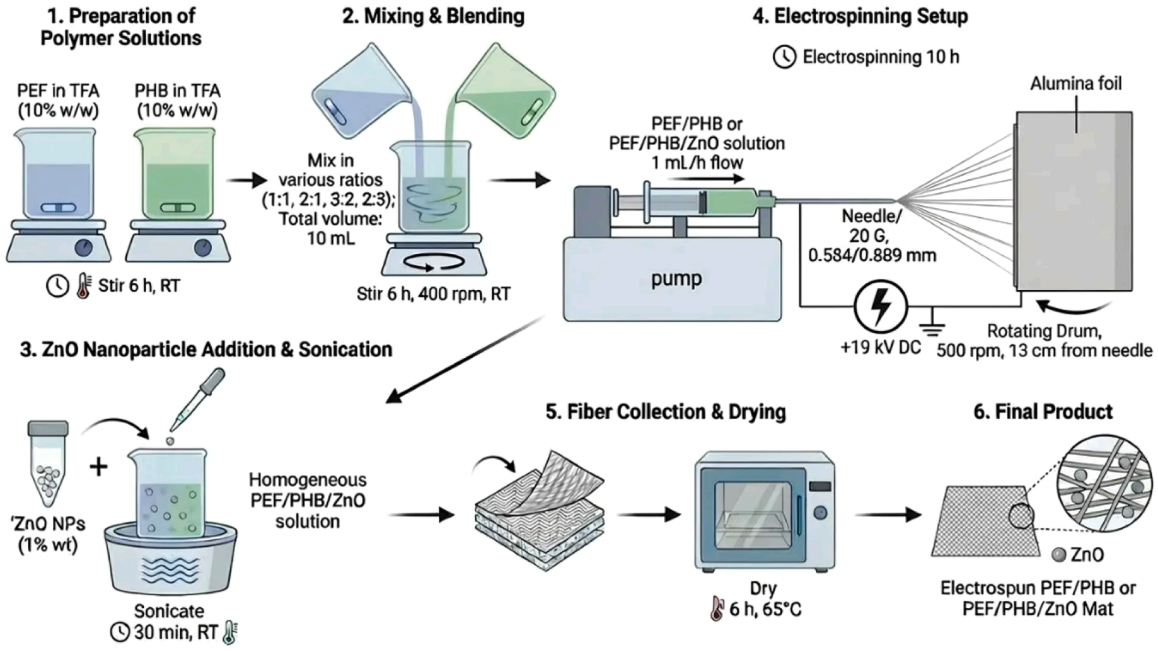

Scheme 1. Schematic representation of the electrospinning process.

(dia~1730 × 30 mm^2 squares, covering a weighing bottle (dia ~17 mm), filled with water (20 mL). An elastic rubber band was used to secure the mat on the bottle neck. The weighing bottle was placed in a desiccator containing silica gel for 24 h at RT. The weight of the bottle with water was measured after 24 h and 48 h. Three replicates were run, and the results were reported as averages. The water vapor permeability (WVP) was calculated as follows:

$$WVP = \frac{w \times b}{A \times t \times \Delta P} \quad (1)$$

Where, W is the weight of the sample (g), b (mm) is the thickness of the sample, and t (s) is the time, A (cm^2) is the area of the bottle mouth, and ΔP is the partial pressure (0.02308 at 25 °C) between the deionized water and the dry atmosphere.

2.5. ZnO release and quantification by ICP-MS

2.5.1. Experimental design for ZnO release

A Box–Behnken response surface design was created using Design Expert software (version 13) to study the effects of pH, temperature, and time on ZnO release from the nanofibers. Each parameter was varied in three values as follows: pH (4.2, 6.6, 9); T (4 °C, 22 °C, 40 °C); and time (3, 7, 11 days). The design generated 15 experimental runs, including center-point repetitions. A complete set of conditions is provided in Table S2.

2.5.2. ZnO extraction and sample preparation

Electrospun nanofibers (5 mg) were cut and placed in 50 mL polypropylene tubes, containing 25 mL of the release medium. The pH of the release medium was adjusted using 1 M HCl or 1 M NaOH. The sealed tubes were incubated at selected temperatures and durations, with gentle periodic shaking to ensure proper contact between the fibers and the solution without damaging the mats. After each run, samples were centrifuged (1000 rpm, 10 minutes) at RT. The supernatant was filtered using a 0.45 μm nylon filter.

To prevent precipitation or adsorption on tube walls, each extract was stabilized by adding 100 μL of 1 M HNO_3. The mixture was gently vortexed for 10 s and filtered through a 0.22 μm PTFE syringe filter to remove residual particulates, and subsequently diluted 1:10 (v/v) with ultrapure water (resistivity ≥ 18.2 MΩ·cm). Calibration standards prepared from a certified Zn stock solution were used to create an external calibration curve in the range of 1–50 μg L^{-1}.

Zinc concentrations were measured using an Inductively Coupled Plasma-Mass Spectrometer (ICP-MS, NexION® 350D, PerkinElmer, USA), monitoring the ^{66}Zn isotope for quantification. An alternative isotope (^{67}Zn) was also monitored periodically to confirm that no matrix-related interferences were present. Procedural blanks (release medium + HNO_3, no fiber) and spiked standards (known Zn concentration added to the release medium) were analyzed at the start and after 8 samples to monitor any instrumental drift or contamination. Final Zn release was reported as the mass of Zn in the sample volume (μg/L).

3. Results and discussion

Generally, polymers are immiscible due to low mixing enthalpy and high entropy. Immiscible polymers are technologically more important and practical in real-life applications compared to miscible polymers, where resultant properties are usually an average of the mixed components. Thermodynamics plays a vital role in the theoretical assessment of the miscibility/immiscibility of two polymers. The calculation of solubility parameter (δ), which is a direct indication of cohesive energy density of the polymers, using the group contributions method, helps in deciding the theoretical miscibility/immiscibility level. The solubility parameter (also called the Hansen solubility parameter) [19] is further divided into polar (δ_p), dispersive (δ_d), and H-bonding (δ_h) components, which altogether sum up to provide a single value of δ. Herein, we utilize methods reported by Hoftyzer and Van Krevelen [20] and by Hoy [19] for systematic estimations of δ_d, δ_p, and δ_h, and for estimating δ for PEF and PHB.

$$\delta^2 = \delta_d^2 + \delta_p^2 + \delta_h^2 \quad (2)$$

$$\text{Where } \delta_d = \frac{\sum F_{d,i}}{V}; \delta_p = \frac{\sqrt{\sum F_{p,i}}}{V}; \delta_h = \sqrt{\frac{\sum E_{h,i}}{V}} \quad (3)$$

$$\Delta\delta = \sqrt{(\delta_2 - \delta_1)^2} \quad (4)$$

which, in the form of individual components is given as follows:

$$\Delta\delta = \sqrt{(\delta_{d2} - \delta_{d1})^2 + (\delta_{p2} - \delta_{p1})^2 + (\delta_{h2} - \delta_{h1})^2} \quad (5)$$

Here, V is the total molar volume determined as the summation of the molar volumes of various functional groups, the calculated group contribution, $F_{d,i}$ ($(MJ.m^3)^{0.5}$/mole), and $F_{p,i}$ ($(MJ.m^3)^{0.5}$/mole) are the dispersive and polar molar attractions, and $E_{h,i}$ (J/mole) represents H-bonding energy.

According to Hoftyzer-van Krevelen, $\Delta\delta < 5MPa^{0.5}$ indicates miscibility, whereas a value >5 $MPa^{0.5}$ indicates the immiscibility of the components. Eq. (5) helps in estimating $\Delta\delta$ using individual components' contributions.

Both PHB and PEF contain carboxylic groups, but PEF contains an additional heterogeneous furan ring. The Hoftyzer-van Krevelen [20] method has a limitation that it can calculate the contribution from the benzene ring; however, it does not account for the furan ring. We added furan ring contribution using Hoy's method [19], in addition to the contributions from CH_2, COO^-, >C=, -CH=, and -O- functional groups. For PHB, CH_3, >C=, CH_2, and OH, groups were used in the calculations. The Δδ of PEF and PHB was found to be 9, confirming theoretical immiscibility (Table 1).

In spite of predicting immiscibility theoretically, there was no evidence of phase separation between electrospun PEF and PHB, owing to the chemical interaction between them (Fig. 2, discussed later). Furthermore, homogenous PEF/PHB blends were revealed in SEM imaging (Fig. 1) without any color changes reflecting any phase separation. Therefore, we conclude that even though PEF and PHB are theoretically immiscible, the group contribution reflects only macroscale miscibility/immiscibility, whereas in nanofibers, this method may not work.

3.1. ZnO-loaded PEF/PHB nanofibers nonwoven mats

The electrospun PEF nonwoven mats exhibited a narrow diameter distribution with a mean average diameter, d_{avg} <100 nm (Fig. 1a), whereas neat PHB showed a higher d_{avg} ~132 nm (Fig. 1b). When blended, there was a characteristic shift in the morphological features in several aspects. Firstly, there was a marked variation in d_{avg}, and a wider fiber diameter distribution was observed (Fig. 1). Optimization of blending proportions was carried out, and the PEF/PHB ratio was changed to 1/1, 2/1, and 3/2. The PEF/PHB 1/1 showed d_{avg} as the average of two components as expected (Fig. 1d). Increasing the PEF concentration in PEF/PHB 2/1 and 3/2 resulted in d_{avg} of 87 nm and 97 nm, respectively. There were big globules of PEF observed in PEF/PHB 2/1, attributed to the self-confinement of PEF and less attraction from PHB towards homogenous dispersion of PEF. The introduction of 1 wt% ZnO nanoparticles increased the d_{avg} to 134 nm (Fig. 1f), which is attributed to stabilized interactions between PEF-ZnO-PHB (Fig. 2g, discussed later).

Furthermore, higher concentration of PHB in the blends increased d_{avg} distribution. Fiber diameter distribution is a complex function of various process and material parameters. Pure PEF mats showed uniform and unbroken fibers with relatively low d_{avg} distribution, whereas blending with PHB led to breaking and discontinuous fibers Fig. 2b and c. It is worth noting that electrospinning pure PHB generated beaded fibers, whereas the beads disappeared when PHB was blended with PEF. Blending of two polymers is often associated with disparities in surface charge and conductivity. The PEF/PHB mats exhibited the formation of Y-branched and discontinuous fibers, resulting from stronger whipping and splitting effects in the spinning jet, which might be attributed to an increase in conductivity and a reduction in surface tension in the blend [20]. The blending of PEF and PHB polymers resulted in the Y-branching of the fibers, which was further enhanced by incorporating filler material into the blend. The resultant Y-branched fiber morphology in blends can be associated with a higher gas/vapor barrier.

Table 1
Molar volume (V) and Solubility parameter (δ).

	V (cm^3/mol)	δ (MPa)	Δδ $(MPa)^{0.5}$
PHB	73.96	15.3	9
PEF	125.67	24.3	

Note: Complete Group contribution method details are provided in Table S1.

The FTIR spectra revealed the interaction between PEF and PHB (Fig. 2a). There was evidence of changes in deformation bending in the range 1400 and 1200 cm^{-1}. PEF being amorphous, does not have any crystalline peak; therefore, the peak at 1760 cm^{-1} was linked to inherent crystallinity of PHB in the blended nanofibers (Fig. 2b). The carbonyl peak at 1720 cm^{-1} changed slightly in shape, which might be attributed to Zn^{2+} and C=O interactions in PEF/PHB blend nanofibers. A stable C—O-C peak in PEF was observed at 1080–1200 cm^{-1} (Fig. 2c). The effects of partially positive Zn^{2+} on C—O-C are more evident compared to its effect on the C=O peak in Fig. 2b. Fig. 2 (e, f, g) show stabilization effects of Zn^{2+} via interactions with the -OH groups in both PEF and PHB. Two separate -OH contributions were observed in PEF/PHB blend (Fig. 2e and deconvoluted -OH peak in Fig. 2f) at 3300–3800 cm^{-1}, evidencing the physical mixing of PEF and PHB. Inclusion of ZnO nanoparticles produced Zn^{2+} that stabilized duel -OH peak in blend fibers into a single -OH peak in PEF/PHB+ZnO (Fig. 2e and deconvoluted spectra Fig. 2g). It is our understanding and hypothesis that Zn^{2+} attached at -OH spot might be difficult to release (discussed later) and it would be challenging for triggers (antimicrobial or antioxidant testing, discussed later) to access Zn nanoparticles.

Dynamic contact angles from 0 s to 10 s were observed for PEF, PHB, neat PEF/PHB, and PEF/PHB+ZnO (Fig. 2h). Since the electrospinning was performed in TFA as solvent, PEF exhibited under 90° water contact angle (WCA) which collapsed within 10 s to 35°, showing a hydrophilic surface. The results agree with Svyntkivska et al. [21] where they used a combination of TFA and HFIP solvents for electrospinning PEF. Similar observations were made by Kandiyil et al. in PEF/PLA co-electrospinning [15]. Interestingly, PEF/PHB blend nanofibers showed an initial contact angle of 75°, which collapsed drastically to 8° in 10 s, which is attributed to the presence of individual hydroxyl groups present in the blends (Fig. 2g). Inclusion of ZnO in fibers usually renders them more hydrophilic, which is similar to what was observed in this study.

PEF nanofibers exhibited higher thermal stability compared to PHB (Fig. 2i) with an onset of degradation (T_{onset}) at 380 °C. T_{onset} for PHB was at 270 °C, in agreement with Panayotidou et al. [22]. In PEF/PHB blend nanofibers, both PEF and PHB exhibited their characteristic decomposition behaviors. The introduction of ZnO slightly improved T_{onset} of the blend, which is attributed to the intercalating and stabilizing interactions observed in Fig. 2g, similar to the stabilization effects observed in [23].

The stress-strain data of the electrospun nonwoven mats are shown in Fig. 3a and Table 2. PHB is considered a brittle polymer with low strain at break (ε_b). Electrospinning results in fast cooling (crystallization) of the spun fibers, which creates ordered lamellae in PHB. PHB showed similar brittle behavior, high initial modulus (E ~17.5 MPa), and low ε_b (17%), in agreement with Sudesh et al. [24]. PEF exhibited a lower modulus (12.8 MPa) but higher ε_b compared to PHB (~28%). Though PEF shows low ε_b in the molded articles [5], the electrospun mats have been shown to be more stretchable depending upon the choice of solvent used during electrospinning PEF [15]. Higher ε_b of PEF can be attributed to the furan-ring, which does not allow close packing, and lamellae are still stretchable. Interestingly, the PEF/PHB blend nanofibers showed lower modulus compared to PHB and PEF but higher ε_b (~35%). This is linked with the increased free volume due to PEF's furan rings, leading to increased amorphous structure. With the inclusion of ZnO, a classical filler-polymer connect-based high modulus, low ε_b material was observed. The reduced ductility in PEF/PHB+ZnO is attributed to pressure points created by ZnO nanoparticles [25] during the stabilization interactions (observed in Fig. 2g).

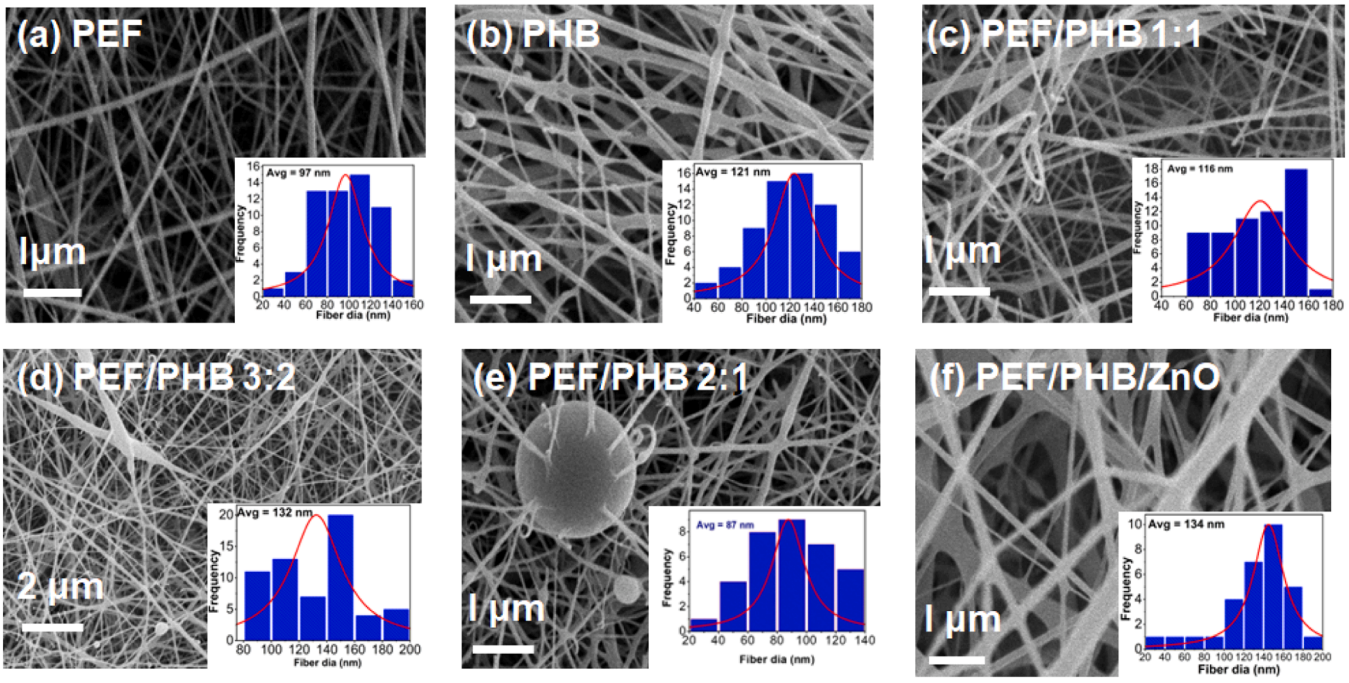

Fig. 1. Nonwoven mats with fiber diameter distribution of a) PEF, b) PHB, c) PEF/PHB 1:1, d) PEF/PHB 3:2, e) PEF/PHB 2:1, and f) PEF/PHB 1:1 +ZnO.

The crystallinity of the spun fibers was studied using XRD. PEF showing a broad peak 15–25° and absence of sharp peaks, indicated an amorphous structure with limited long-range [26]. PHB showed sharp peaks at lower 2θ between 12–25°, showing its semi-crystalline structure with sharp scattering from (020) and (110) of the orthorhombic unit cell at 12° and 17°, respectively. Peaks at 21° and 22° correspond to (101) and (111) α-planes of the PHB crystals (Fig. 3b) [27]. Thanh et al. reported that PHB electrospun nanofibers have a reduction in β-crystal reflections compared to the PHB films [8]. In PEF/PHB blends, the peaks in the lower 2θ originate from neat PHB, whereas the broad PEF peak disappeared. We attribute this pattern to the induced amorphous structure in the blend due to free volume associated with furan rings in PEF, leading to high elongation at break and lower modulus in agreement with mechanical testing (Table 2). Neat ZnO nanoparticles exhibited a highly crystalline, hexagonal wurtzite structure with phase purity. ZnO totally diminished PHB's crystalline peaks largely due to the interference of the reduced chain packing in PEF/PHB+ZnO fibers [28].

4. Release of the embedded-ZnO: factors and mechanism

The release of ZnO from the PEF/PHB electrospun nonwoven mats was evaluated as Zn^{2+} to understand the effects of pH, T, and t on the release rate. A Box–Behnken response surface model (Eq. (6)) revealed that all three factors [T(A), pH (B), and t (C)] significantly affected Zn^{2+} release ($p < 0.05$). The R^2 of 0.99 and adjusted R^2 of 0.977 of the fitted model (Fig. 4a-c) indicate a linear relation between T and release rate, whereas pH and time showed inverse relations. The significant quadratic terms (B^2, C^2) indicate curvature in the response surface, suggesting that these factors have an optimal operating range rather than a simple linear trend. Moreover, the interaction terms (AB and AC) demonstrate that the effect of pH (B) and time (C) depended on T (Fig. 4d-e). Overall, the model confirms that Zn^{2+} release increases with higher temperatures and decreasing pH, consistent with the release behavior predicted by Eq. (6):

$$Zn^{2+} = 8.38 + 0.7433A - 5.36B - 0.6056C - 0.7785AB + 1.15AC + 0.4250BC + 0.6536A^2 - 3.50B^2 + 1.42C^2 \quad (6)$$

The substantial increase in Zn^{2+} at low pH (Fig. 4d) is attributed to increased acidity that drives the leaching reaction forward by promoting separation of nanofibers in the nonwoven mat (Fig. 5), in agreement with ref [29]. As pH increases, more negatively charged functional groups (–OH, $–COO^-$, $–O^-$) form in the matrix, creating additional binding sites that strongly attract Zn^{2+} and limit its release. A pH of 5.32 is the optimal pH determined by the model for higher intended Zn^{2+} release. In addition, higher T at lower pH increases the desorption of Zn^{2+} (Fig. 4e and 5). Extended extraction time led to a slight reduction in Zn release initially, with subsequent increase with time. This may result from surface passivation, where products such as Zn hydroxide or carbonate form a protective layer that slows further dissolution. Additionally, ZnO particle aggregation over time can reduce available surface area for interaction with the solvent, lowering extraction efficiency.

In order to explain the effect of pH on the fiber morphology, we studied the morphology of PEF/PHB and PEF/PHB+ZnO nonwoven mats at high (basic) and low (acidic) pH. Interestingly, d_{avg} increased in PEF/PHB nonwoven mats from 116 nm to 130+ nm under both acidic and basic conditions, attributed to the merging of small fibers (Fig. 5a1-a2). The d_{avg} in PEF/PHB+ZnO nonwoven mats (d_{avg}~132 nm) decreased significantly to 90 nm under acidic pH (Fig. 5b1), whereas a d_{avg}~110 nm was observed under basic conditions (Fig. 5b2). These results show that Zn^{2+} release is also linked with the fiber diameter in addition to the pH alone. However, these effects need separate systematic investigation.

Fig. 6a shows the effects of basic and acidic environments on the dynamic WCA. In neat PEF/PHB nonwoven mats, the initial WCA decreased from 75° (acidic) to 32° (basic), which decreased to 35° (acidic) and 22° (basic) after 10 s. Interestingly, no significant difference was observed in PEF/PHB+ZnO nonwoven mats under acidic or basic conditions. The electrospun nonwoven mats were examined for water vapor permeability (WVP). Neat PEF nonwoven mats exhibited the lowest WVP after 24 h. The neat PHB, PEF/PHB, and PEF/PHB-ZnO nonwoven mats exhibited higher moisture diffusion, attributed to the hydrophilic nature of PHB (Fig. 6b). The nonwoven mats showed very low water permeation in 24 h through the films. Highest water permeation was observed in PEF/PHB+ZnO nonwoven mats after 48 h, which is a direct indication of the rose petal effect, but was not observed in

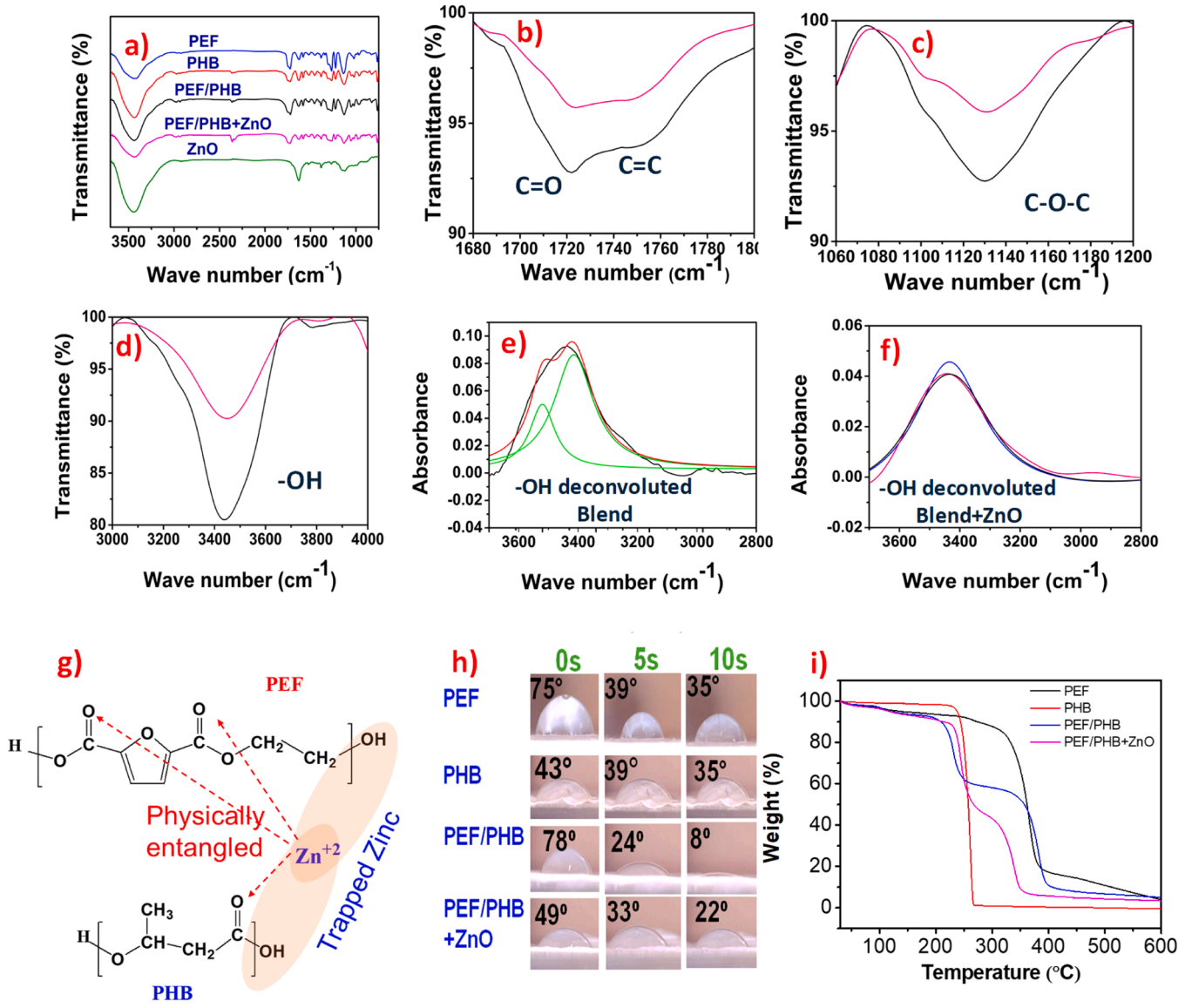

Fig. 2. FTIR spectra of a) nonwoven mats and ZnO, b-f) extrapolations and deconvolution of FTIR spectra g) schematics of Zn interactions h) WCA of mats, and i) thermal stability.

WCA.

We also investigated the antimicrobial and antioxidant properties of the developed nonwoven mats since ZnO is widely reported for its strong antibacterial properties. Several tests to assess the antibacterial properties were performed using disc diffusion and CFU techniques. There were no significant results observed owing to the entrapment of Zn^{2+} within the matrix. Similarly, we performed the DPPH radical scavenging test to understand the antioxidant properties of the nonwoven mats. The ZnO-loaded mats exhibited a slightly higher value than the neat PEF/PHB blends (6% vs 3%), which were below 10% efficiency, regarded as insignificant antioxidant results. Therefore, we conclude with confidence that when Zn^{2+} nanoparticles are trapped inside the matrix, and their release is limited, there is less or no exposure of Zn^{2+} to the bacterial strains and DPPH radicals, leading to biological properties.

5. Conclusion

Novel nonwoven membranes of 100% biobased PEF/PHB+ZnO were co-electrospun together. Both PEF and PHB were theoretically predicted to be immiscible, as revealed by a solubility parameter difference of 9. However, the co-spun fibers exhibited no phase separation. ZnO further stabilized PEF-PHB interactions, indicated by a stable -OH peak in PEF/PHB+ZnO nonwoven mats. PEF was hydrophobic, whereas PHB was hydrophilic; the blend mats were almost hydrophobic, but became hydrophilic upon addition of ZnO. The hydrophilic behavior of the nonwoven mats as a function of time revealed the inverse of 'the rose petal effect'.

The nonwoven mats showed no significant biological properties, owing to the significant entrapment of ZnO within the PEF/PHB fibers, stabilizing polymer-Zn^{2+}-polymer interactions. This stabilization was further evidenced by increased modulus and tensile strength of PEF/PHB+ZnO mats. The current study opens a new venue where Zn^{2+} release could be controlled via pH and temperature. Moreover, insights gained from this study would be critical for future formulations of nano-loaded electrospun nanofibers to harness their full potential in the food packaging industry.

Declaration of generative AI and AI-assisted technologies in the manuscript preparation process

During the preparation of this work the authors used Graphic AI Tool (Figure Lab AI) in order to enhance and improve quality of Schematic-1

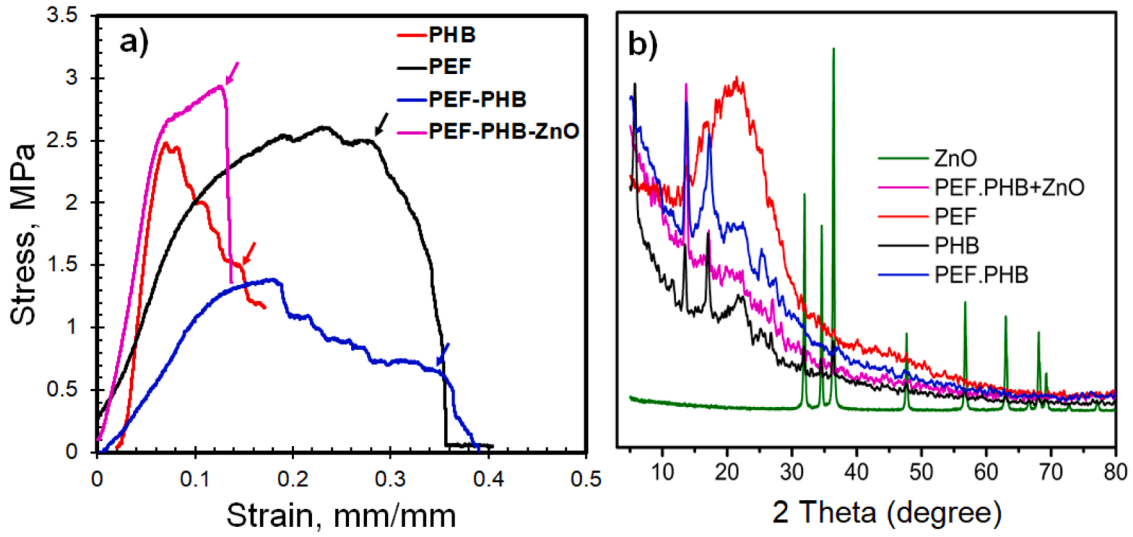

Fig. 3. Mechanical properties a) and XRD pattern of composite nanofibers.

Table 2
Young's modulus (E), tensile strength (TS), and elongation at break (ε_b) for electrospun mats.

Sample	E (MPa)	TS (MPa)	ε_b (%)
PHB	17.5	2.5	17.1
PEF	12.8	2.5	28
PEF/PHB	9.3	1.25	35.2
PEF/PHB+ZnO	30.2	3.0	12.7

and Graphical Abstract. After using this tool, the authors reviewed and edited the content as needed and take full responsibility for the content of the published article.

CRediT authorship contribution statement

James Kegere: Writing – original draft, Investigation, Formal analysis, Data curation, Conceptualization. **Athira V. Aramughan:** Writing – original draft, Investigation, Data curation. **Anuj Niroula:** Methodology, Data curation. **Bismi Phasaludeen:** Methodology, Data curation. **Akmal Nazir:** Writing – review & editing, Supervision, Resources, Project administration, Funding acquisition, Conceptualization. **Ioannis Zuburtikudis:** Writing – review & editing, Project administration, Funding acquisition. **Muhammad Z. Iqbal:** Writing – review & editing, Writing – original draft, Supervision, Resources, Project administration, Funding acquisition, Conceptualization.

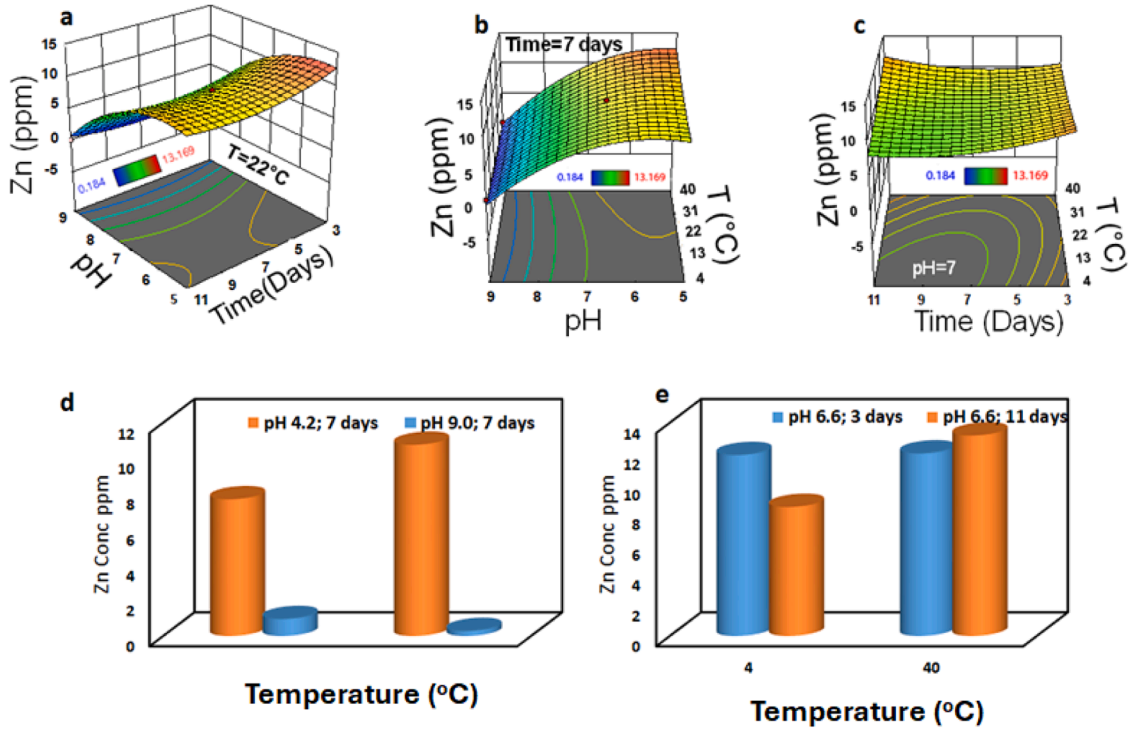

Fig. 4. Embedded-ZnO release concentration profiles (a) effect of pH as a function of time at fixed temperature (b) effect of pH as a function of temperature at fixed time (c) effect of temperature against time at fixed pH, while (d and e) are combined effect of time and pH at varied temperature conditions.

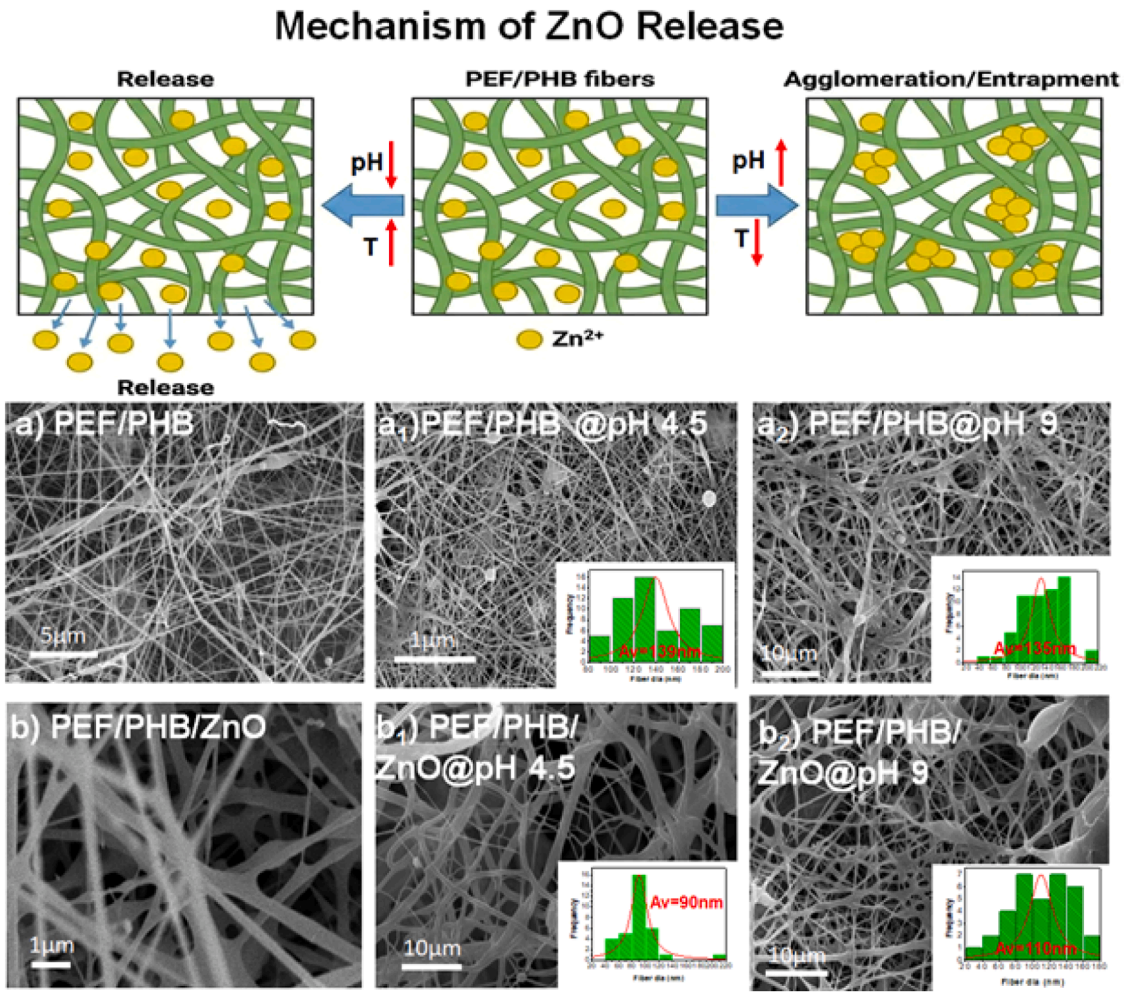

Fig. 5. Mechanism of Zinc release, Neat blend nonwoven mats (a,b) and effects of acidic (a_1, b_1) and basic pH (a_2, b_2).

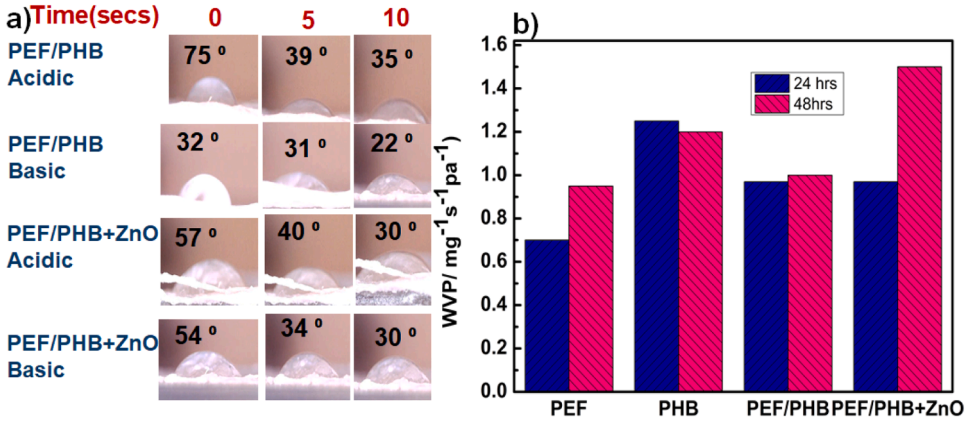

Fig. 6. WCA of blend nonwoven mats surface under acidic and basic environment a), and water vapor permeation rates b), mechanical properties.

Declaration of competing interest

Authors declare that there is no conflict of interest related to this work.

Acknowledgements

Authors acknowledge the funding received through Abu Dhabi University-United Arab Emirates University (ADU-UAEU) joint research program in grant 12N139 and partial support from grant 12N002 under the UAEU Program for Advanced Research. The authors acknowledge and appreciate discussions with Prof. Muhammad Tahir on the zinc entrapment and release study.

Supplementary materials

Supplementary material associated with this article can be found, in the online version, at doi:10.1016/j.rineng.2026.110781.

Data availability

Data will be made available on request.

References

[1] N. Poulopoulou, et al., Green polymeric materials: on the dynamic homogeneity and miscibility of furan-based polyester blends, Polymer 174 (2019) 187–199, https://doi.org/10.1016/j.polymer.2019.04.058.

[2] E. Panayotidou, A. Kroustalli, A. Baklavaridis, I. Zuburtikudis, D.S. Achilias, D. Deligianni, Biopolyester-based nanocomposites: structural, thermo-mechanical and biocompatibility characteristics of poly(3-hydroxybutyrate)/montmorillonite clay nanohybrids, J. Appl. Polym. Sci. 132 (2015), https://doi.org/10.1002/app.41628.

[3] G. Göksen, M.J. Fabra, A. Pérez-Cataluña, H.I. Ekiz, G. Sanchez, A. López-Rubio, Biodegradable active food packaging structures based on hybrid cross-linked electrospun polyvinyl alcohol fibers containing essential oils and their application in the preservation of chicken breast fillets, Food Packag. Shelf Life 27 (2021), https://doi.org/10.1016/j.fpsl.2020.100613.

[4] S. Thongkham, Environmentally friendly nanomembrane from PEF-PHBv composites: preparation and investigation of morphologies, thermal, and mechanical properties, Res. Square (2023), https://doi.org/10.21203/rs.3.rs-3673950/v1.

[5] S. Ahmed, R. Cardinaels, B. Abu-Jdayil, A. Munam, M.Z. Iqbal, Engineering the interface of interfacially-locked graphene in electrically conductive poly (ethylene furanoate)/polyethylene (PEF/PE) blends, Macromol. Mater. Eng. (2025), https://doi.org/10.1002/mame.202500177.

[6] O. Olejnik, A. Masek, J. Zawadziłło, Processability and mechanical properties of thermoplastic polylactide/polyhydroxybutyrate (PLA/PHB) bioblends, Materials (2021) 1–12, https://doi.org/10.3390/ma14040898.

[7] S.K. Burgess, J.E. Leisen, B.E. Kraftschik, C.R. Mubarak, R.M. Kriegel, W.J. Koros, Chain mobility, thermal, and mechanical properties of poly(ethylene furanoate) compared to poly(ethylene terephthalate), Macromolecules 47 (2014) 1383–1391, https://doi.org/10.1021/ma5000199.

[8] N.H. Thanh, R. Olekhnovich, V. Sitnikova, A. Kremleva, P. Snetkov, M. Uspenskaya, PHB/PEG nanofiber mat obtained by electrospinning and their performances, Technologies 11 (2023), https://doi.org/10.3390/technologies11020048.

[9] A. Rohani Shirvan, N. Hemmatinejad, S.H. Bahrami, A. Bashari, A comparison between solvent casting and electrospinning methods for the fabrication of neem extract-containing buccal films, J. Ind. Text. 51 (2022) 311S–335S, https://doi.org/10.1177/15280837211027785.

[10] K. Molnar, L.M. Vas, T. Czigany, Determination of tensile strength of electrospun single nanofibers through modeling tensile behavior of the nanofibrous mat, Comp. B: Eng. (2012) 15–21, https://doi.org/10.1016/j.compositesb.2011.04.024.

[11] C. Del Gaudio, E. Ercolani, F. Nanni, A. Bianco, Assessment of poly (ε-caprolactone)/poly(3-hydroxybutyrate-co-3-hydroxyvalerate) blends processed by solvent casting and electrospinning, Mater. Sci. Eng.: A 528 (2011) 1764–1772, https://doi.org/10.1016/j.msea.2010.11.012.

[12] A. Bahrami, R. Delshadi, E. Assadpour, S.M. Jafari, L. Williams, Antimicrobial-loaded Nanocarriers for Food Packaging Applications, Elsevier B.V, 2020, https://doi.org/10.1016/j.cis.2020.102140.

[13] J. Ding, et al., Large-size ultrathin mica nanosheets: reinforcements of biobased PEF polyester, Giant 18 (2024), https://doi.org/10.1016/j.giant.2024.100264.

[14] S. Ahmed, R. Cardinaels, B. Abu-Jdayil, A. Munam, M.Z. Iqbal, Toughening brittle poly(ethylene Furanoate) with linear low-density polyethylene via interface modulation using reactive compatibilizers, ACS Omega 10 (2025) 5756–5769, https://doi.org/10.1021/acsomega.4c09301.

[15] K. Juraij, A. Niroula, Y. Greish, P.K.S. Mural, A. Nazir, M.Z. Iqbal, Sustainable, antifouling poly (ethylene furanoate)/poly (lactic acid) (PEF/PLA) blend electrospun nanofibrous membranes for switchable premix emulsification/demulsification, J. Memb. Sci. 717 (2025), https://doi.org/10.1016/j.memsci.2024.123622.

[16] F.S. Jebel, H. Almasi, Morphological, physical, antimicrobial and release properties of ZnO nanoparticles-loaded bacterial cellulose films, Carbohydr. Polym. 149 (2016) 8–19, https://doi.org/10.1016/j.carbpol.2016.04.089.

[17] S. Amjadi, S. Emaminia, S. Heyat Davudian, S. Pourmohammad, H. Hamishehkar, L. Roufegarinejad, Preparation and characterization of gelatin-based nanocomposite containing chitosan nanofiber and ZnO nanoparticles, Carbohydr. Polym. 216 (2019) 376–384, https://doi.org/10.1016/j.carbpol.2019.03.062.

[18] L.K. Kurabetta, et al., A synergistic influence of gallic acid/ZnO NPs to strengthen the multifunctional properties of methylcellulose: a conservative approach for tomato preservation, Int. J. Biol. Macromol. 277 (2024), https://doi.org/10.1016/j.ijbiomac.2024.134191.

[19] V.G. Bhat, S.S. Narasagoudr, S.P. Masti, R.B. Chougale, A.B. Vantamuri, D. Kasai, Development and evaluation of Moringa extract incorporated Chitosan/Guar gum/Poly (vinyl alcohol) active films for food packaging applications, Int. J. Biol. Macromol. 200 (2022) 50–60, https://doi.org/10.1016/j.ijbiomac.2021.12.116.

[20] R. Liu, et al., Tetrabutylammonium chloride triggered polyvinylidene fluoride - thermoplastic polyurethane branched-nanofiber films for air filtration, J. Memb. Sci. 719 (2025), https://doi.org/10.1016/j.memsci.2025.123739.

[21] M. Svyntkivska, T. Makowski, E.L. de Boer, E. Piorkowska, Solution electrospinning and properties of poly(ethylene 2,5-furandicarboxylate) fibers, Polym. Test. 113 (2022), https://doi.org/10.1016/j.polymertesting.2022.107677.

[22] E. Panayotidou, A. Baklavaridis, I. Zuburtikudis, D.S. Achilias, Nanocomposites of poly(3-hydroxybutyrate)/organomodified montmorillonite: effect of the nanofiller on the polymer's biodegradation, J. Appl. Polym. Sci. 132 (2015), https://doi.org/10.1002/app.41656.

[23] M. Râpă, et al., Electrospun nanosystems based on PHBV and ZnO for ecological food packaging, Polymers 13 (2021), https://doi.org/10.3390/polym13132123.

[24] K. Sudesh, H. Abe, Y. Doi, Synthesis, structure and properties of polyhydroxyalkanoates: biological polyesters, Prog. Polym. Sci. 10 (2000) 1503–1555, https://doi.org/10.1016/S0079-6700(00)00035-6.

[25] S.Y. Fu, X.Q. Feng, B. Lauke, Y.W. Mai, Effects of particle size, particle/matrix interface adhesion and particle loading on mechanical properties of particulate-polymer composites, Compos. B Eng. 39 (2018) 933–961, https://doi.org/10.1016/j.compositesb.2008.01.002.

[26] K. Su, W. Luo, B. Xiao, Y. Weng, C. Zhang, Advancements in the Crystallization and Regulation of Poly(ethylene 2,5-furandicarboxylate) (PEF): A review, Elsevier B.V, 2025, https://doi.org/10.1016/j.indcrop.2024.120184.

[27] D.A. D'Amico, L.B. Manfredi, V.P. Cyras, Crystallization behavior of poly(3-hydroxybutyrate) nanocomposites based on modified clays: effect of organic modifiers, Thermochim. Acta 544 (2012) 47–53, https://doi.org/10.1016/j.tca.2012.06.012.

[28] X. Wen, W. Zhao, Y. Su, D. Wang, Interfacial Effects on Crystallization Behavior of Polymer Nanocomposites with Polymer-Grafted Nanoparticles, John Wiley and Sons Inc, 2019, https://doi.org/10.1002/pcr2.10066.

[29] F. Soltani, H. Darabi, R. Aram, M. Ghadiri, Leaching and solvent extraction purification of zinc from Mehdiabad complex oxide ore, Sci. Rep. 11 (2021) 1566. https://www.nature.com/articles/s41598-021-81141-7.